October 2021

Synthesis of Hybrid Inorganic-Organic Microparticles

Shreyas Joshi

Synthesis of Hybrid Inorganic-Organic Microparticles

Shreyas Joshi

SYNTHESIS OF HYBRID INORGANIC-ORGANIC MICROPARTICLES

A Thesis Presented

by

SHREYAS JOSHI

Submitted to the Graduate School of the
University of Massachusetts Amherst in partial fulfillment
of the requirements for the degree of

MASTER OF SCIENCE IN CHEMICAL ENGINEERING

September 2021

Chemical Engineering

SYNTHESIS OF HYBRID INORGANIC-ORGANIC MICROPARTICLES

A Thesis Presented

By

SHREYAS JOSHI

Approved as to style and content by:

DocuSigned by:

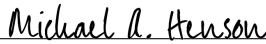*Peter Beltramo*

Peter J. Beltramo, Chair

DocuSigned by:

John Klier

John Klier, Member

DocuSigned by:

Kevin Kittilstved

Kevin Kittilstved, Outside Member

DocuSigned by:

Michael A. Henson

Michael Henson, Department Head
Chemical Engineering

ABSTRACT

SYNTHESIS OF HYBRID INORGANIC-ORGANIC MICROPARTICLES

SEPTEMBER 2021

SHREYAS JOSHI, B.E. UNIVERSITY OF MUMBAI,

M.S. UNIVERSITY OF MASSACHUSETTS AMHERST

Directed by: Professor Peter J. Beltramo

The self-assembly of isotropic and anisotropic colloidal particles into higher-ordered structures has been of great interest recently due to the promise of creating metamaterials with novel macroscopic properties. The physicochemical properties of these metamaterials can be tailored to achieve composites with tunable functionalities. The formation of these metamaterials can be used as a pathway to emulating advanced biological systems. In particular, synthetically mimicking the surface of a moth's eye, which consists of arrays of ellipsoidal protuberances, can be used as a strategy for fabricating antireflective coatings.

To enable this technology, it is necessary to design a synthesis scheme that produces micron-sized composite particles with tunable refractive index. In the future, the resulting composite microparticles can then undergo geometric and spatial modifications to form self-assemblies that have unique macroscopic material properties. This research work delineates a strategy of developing microparticles with a hybrid configuration that constitutes an inorganic and an organic part. The inorganic part comprises ~30 nm diameter titania (TiO_2)

nanoparticles, which are embedded within an organic polymer particle comprised of diethyl methylene malonate polymer [p(DEMM)]. Anionic polymerization is modified to controllably incorporate TiO_2 nanoparticles into the polymer matrix. A design of experiments was identified and carried out to identify the major process variables that influence the final particle size. In particular, since DEMM polymerization may be initiated entirely by the presence of hydroxyl anions, pH was found to control the final overall particle diameter between 300 nm and 1 micrometer. The overall inorganic particle loading can be readily modified and is confirmed by thermogravimetric analysis, allowing for the desired macroscopic refractive index to be controlled. Light scattering, scanning electron microscopy and zeta potential analysis reveals that the colloidal stability of the hybrid microparticles is dependent on the ligand coating the inorganic constituent. In addition, this synthetic scheme is applied to different inorganic constituents that have interesting functionalities, such as fluorescent CdTe quantum dots, in order to show the methods versatility method to produce composite particles for a wide spectrum of applications. These initial investigations provide a the synthetic groundwork to evaluating the coating properties of the microparticles and their self-assembly into novel materials in the future.

TABLE OF CONTENTS

LIST OF FIGURES

CHAPTER 1

Introduction

The coatings industry constitutes a billion-dollar market in the U.S and is predicted to be on the ascent in the coming years. This rising demand along with technological advancements necessitate the development of coatings with controllable functionalities that can drive the wide applications space. Nanoscale inorganic constituents that have favorable properties for particular applications can be incorporated into a microscale organic polymer component to result in a composite material with enhanced macroscopic functionality. The strategy of developing composite systems for advanced applications has already shown promise in a range of applications.   [1] For instance, titania (TiO_2) nanoparticles (NPS) modified by polyacrylic acid show properties of molecular recognition and are used in the synthesis of drug delivery systems to kill cancer cells. The TiO_2 NPs have photocatalyst properties and are used to enhance the hydroxyl (OH) radical generation by ultrasound irradiation.[2], [3] Antimony-based hybrid organic-inorganic materials have shown improvement in the efficiency and stability of the polymer solar cells.[4] A novel method for coating diethyl-5-hydroxyisophthalate (DEIP) as an organic coating on ZrO_2, SiO_2, TiO_2 nanoparticles using electron transfer technique gives self-cleaning and anti-corrosive properties to the metallic surfaces.[5]   These hybrid organic-inorganic configurations can be used effectively to construct systems with tunable functionalities which can further be transformed into coatings by sol-gel or lithographic techniques.

A similar synthetic strategy is designed to fabricate metamaterial systems that serve as the feedstock material for developing anti-reflective coatings. An inorganic-organic configuration as discussed above is used for achieving the antireflective properties. The

idea originates from biomimetics where we intend to emulate the surface patterns seen in the surface of a moth's eye. The goal of this research work is to develop microparticles of hybrid inorganic-organic microstructure, as synthetic counterparts of the biological protuberances that can be self-assembled to form a monolayer with antireflective properties.

1.1 Biomimetics for developing anti-reflective coatings

Existing biomolecular systems have advanced properties which can be synthetically replicated to prepare metamaterials with a tailorable functionality. These biomimetic adaptations are used for constructing materials with applications in biomaterial synthesis, micro-optics, coating technologies, and photovoltaics. In particular, it is desired is to develop coatings that have a uniform gradience in the refractive index (RI) as a function of the layer thickness for imparting antireflectivity.
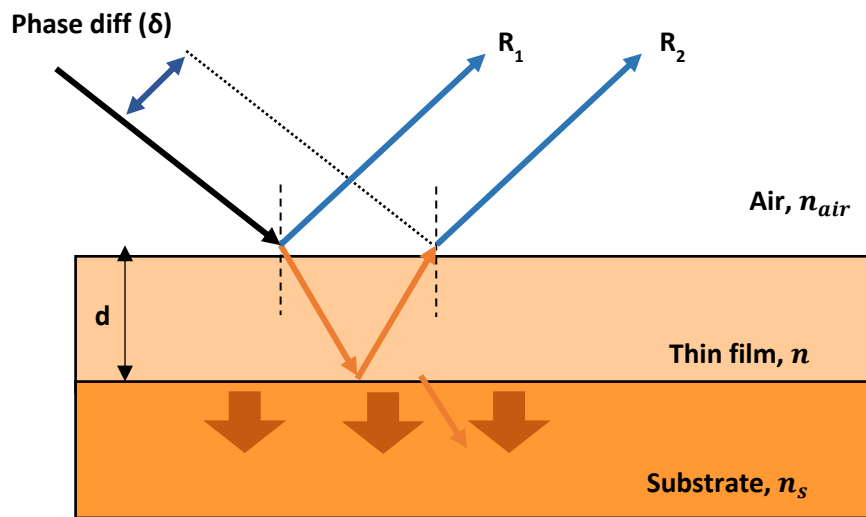
Fig. 1.1: Interaction of light rays with an AR single layer coating leading to destructive interference.

Light rays undergo reflection and refraction as they travel from one medium to another due to the change in the material property, known as the refractive index. The index-matching or optical impedance matching is a technique used to develop surfaces with graded RI that lead to the minimization of the reflection of the incident light. The reflected light rays from a surface with graded RI are π radians out of phase with the incident light rays (Fig.1.1). This causes a destructive interference between the two light rays thereby canceling each other, leading to no reflection. If only a single homogeneous coating material is used, the refractive index should be the geometric mean of the refractive index of the air (n_{air}) and the substrate (n_s), $(n = \sqrt{n_{air} n_s})$. Also, the thickness of the coating material (d) should be an odd multiple of $\lambda/4$, where λ is the wavelength of the incident light. However, the material will only be maximally antireflective at the single wavelength λ and not over a broadband of incident light. However, these optical interactions can be exploited to develop a robust strategy for forming graded RI coatings either from many layers or a single layer with a particular geometry, as explained next.

1.1.1 Characteristics of perfect anti-reflectivity

It is challenging to develop a coating with a perfect anti-reflective property. The angle of incidence, the wavelength of the incident light rays, the polarization of the light are the major factors that influence the anti-reflective property of a coating. A coating should have the following characteristics to exhibit high anti-reflectivity.

A) Broadband anti-reflectivity

The anti-reflectivity of a coating must be consistent over a broader spectral range of the incident radiation with varying wavelengths. An optical impedance matching is a process

of furnishing a smooth transition between two mediums with different refractive indices. This results in minimizing the loss of light due to reflection. However, the matching in the visible region of the incident light does not ensure a match in the ultraviolet (UV) or the near-infra-red (NIR) region. This impairs the performance of some anti-reflective coatings in the UV or NIR regions. It is thus critical to develop a coating strategy that accounts for the varying wavelength of the incident radiation.

B) Omnidirectional anti-reflectivity

It has been established by Fresnel that the angle of incidence plays a decisive role in the determination of reflectance. Most glasses and plastics with RI around 1.5 show a 4% reflectance at normal incidence but a 100% reflectance at grazing angles. This same phenomenon is observed in anti-reflective films and numerous designs catering to incident angles from 30º to 60º to the normal.[6][7]

C) Polarization insensitivity

The effect of the two types, s and p polarization of light on the coatings also needs analysis. The s-polarization has the electric field perpendicular to the incidence plane and p-polarization has the electric field parallel to the incidence plane. Polarization plays a very important role in antiglare coatings (AGCs) and anti-reflective coatings (ARCs) since light reflecting at shallow angles has the p-polarized light reflecting the maximum.

1.1.2 Strategies for achieving anti-reflective surfaces.

The previous research work concerning the development of anti-reflective coatings involves the fabrication of composite layers of materials with different RI. These layers are stacked one upon the other to develop a multilayered gradient refractive index surface.[8]

In order to have a larger optical bandwidth for anti-reflectivity, a higher number of materials are stacked together. The thickness and cost of the resulting composite coating is a limiting factor for the number of materials that can be used for its development as it hinders the applicability and economic feasibility of these coatings [9]. The trade-off between a larger bandwidth and the overall applicability renders the multi-layer composite surfaces inefficient for scale-up.

On the other hand, Moghal. et.al synthesized a single layer of silica (PSi) nanoparticles on a polymer substrate for developing coatings with antireflective functionality. Mesoporous silica nanoparticles were mixed with tetraethyl orthosilicate which acts as a binder. The composite chemistry is then coated on a polycarbonate substrate using dip-coating. The formed coating has excellent abrasion resistance and a capability of reducing the reflectance to sub 1% [10]. However, as it is a single-layered coating, it lacks broadband anti-reflectivity. Also, local gradients in the RI are measured with respect to the cross-section of the coating that is not tunable. An alternate strategy is to use porosity for RI gradience. Porous silicon (PSi) is chemically etched on a silicon substrate to form graded RI coatings[8], [11], [12]. A modest reflectance of 3% with other properties of broadband anti-reflectivity, mechanical durability, chemical inertness, abrasion resistance was recorded.[8] However, the drawback of developing porous gradient antireflective surfaces is the lack of porosity control and high-cost manufacturing.

In addition, highly functional nanostructures may be imprinted on a substrate to form antireflective coatings. The geometry of these nanostructures results in the variation of RI as a function of their height. These surfaces can be applied to optical devices like display screens, light-emitting diodes, solar cells, etc. Sun et.al. fabricated sub-wavelength

patterned structures with nano-scale protuberances with a nickel mold on polycarbonate substrate using roll-to-plate (R2P) ultraviolet nanoimprint lithography. The reflectance was from the range of 1-4 % of the incident light for a wide range of angles in the visible light spectrum.[13] Our strategy involves first the synthesis of hybrid particles with the desired composition (the main goal of this thesis), and then the bottom-up assembly of such particles into the desired microstructures without the use of molds. In particular, the fabrication of a surface with arrays of high RI nanostructures, emulating the highly sophisticated biological systems present in the surface of a moth's eye, would achieve this outcome.

1.1.3 Moth-eye configuration for uniform gradience in RI
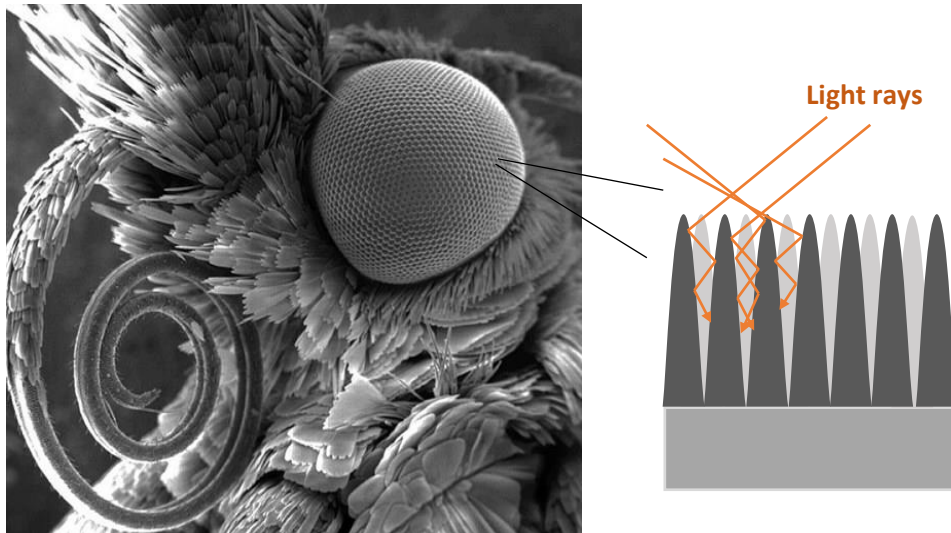
Fig. 1. 2: Moth-eye patterned surface with magnified view of the surface topology.

The surface of a moth's eye has a unique morphology that is developed to evade predators from identifying its location in the dark. It consists of an array of submicron-sized cuticular protuberances that are responsible for diminishing the reflection of the incident light [14]. Light rays are reflected and scattered when incident on a macrostructure

after being partially absorbed. These protuberances comprise of high refractive index material that has an ellipsoid-like configuration (Fig 1.2).
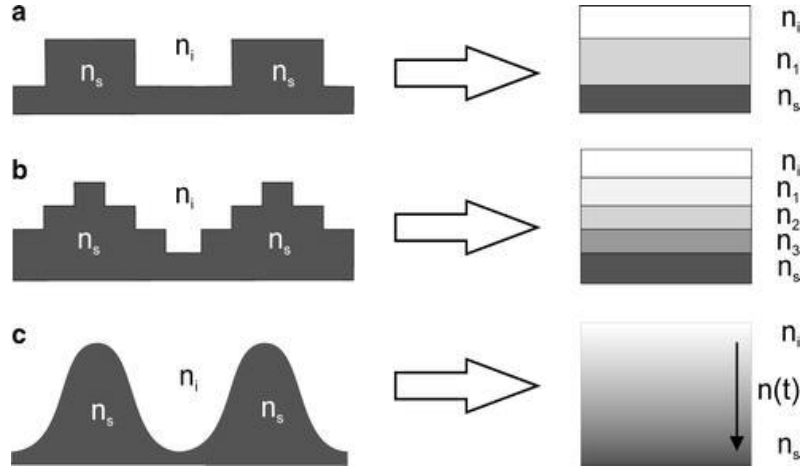
Fig. 1. 3: Gradience in refractive index arising due to the geometry of the protuberances. [15]

The interaction of light is different when incident on structures with dimensions less than its wavelength (sub-wavelength). As light travels through the medium it treats the surface layer-by-layer (Fig. 1.3) since the wavelength of light is greater than the dimensions of the structures forming the arrays. Each infinitesimally thin horizontal layer has a specific effective refractive index value that is a function of the volume fraction of the high RI material occupying the corresponding layer. This forms a medium with continuous refractive index gradation from the top of the surface towards the bottom. Fig. 1.3c shows a uniform gradation in refractive index as a function of the surface thickness resulting due to the semi-ellipsoidal-like geometry of the protuberances. We can emulate this optical phenomenon by synthetically mimicking the moth-eye surface, forming arrays of high refractive index microparticles. This can be achieved by a bottom-up approach of the self-assembly of high refractive index microparticles. [15]

7

1.2 Hybrid Organic/Inorganic microparticles with gradient refractive index

The first step to fabricating antireflective coatings is the synthesis of microparticles with anti-reflective properties. The formation of these hybrid systems requires the use of specific materials that meet the structural and compositional requirements for achieving properties like that seen in the moth's eye. The composition of the resulting hybrid microparticles influences the overall refractive index and thus its optical functionality. The effective refractive index of a composite microparticle can be determined by two models based on the Effective Medium Approximations namely, Bruggeman Approximation and Maxwell-Garnett Model .

Maxwell-Garnett Model	Bruggeman Approximation
$$\left(\frac{n^2 - n_1{}^2}{n^2 + 2n_1{}^2}\right)^2 = (1 - f_1)\left(\frac{n^2 - n_1{}^2}{n^2 + 2n_1{}^2}\right)^2$$	$$f_1\left(\frac{n_1{}^2 - n^2}{n_1{}^2 + 2n^2}\right)^2 = f_2\left(\frac{n_2{}^2 - n^2}{n_2{}^2 + 2n^2}\right)^2$$
Assumption: n₂ is the surrounding phase while n₁ being the dispersed phase	**for k constituents:** $$f_1\left(\frac{n_1{}^2 - n^2}{n_1{}^2 + 2n^2}\right)^2$$ $$- \sum_{i=2}^{k} f_i\left(\frac{n_1{}^2 - n^2}{n_1{}^2 + 2n^2}\right)^2$$

Table 1.1: MG Model vs Bruggeman Approximation for estimating the effective refractive index of the composite system.

Effective Refractive Index vs Mass Fraction of TiO$_2$
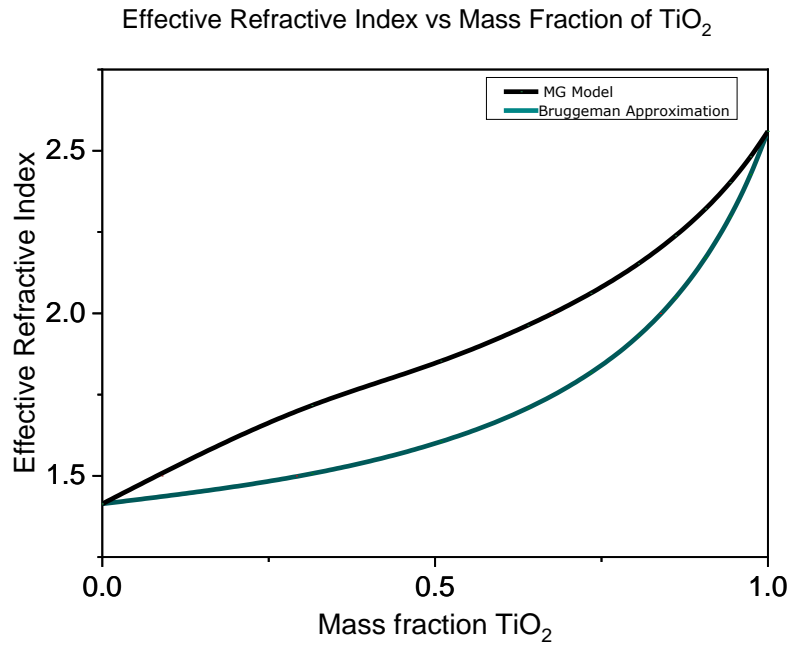
Fig. 1. 4: Maxwell-Garnett model and Bruggemann Approximation for evaluating the effective RI of the composite particles

These models have been derived analytically by averaging the multiple values of the constituents of the composite material. The MG model was derived for evaluating the dielectric constant of the composite materials which was translated to optical applications by relating dielectric constant with the optical permittivity of the composite material. The model though does not take into account the effects of change in geometries of the dispersed constituents that keep the volume fraction fixed and also the parameters of the matrix or the surrounding phase enter the equation not in the same way as that of the dispersed phase and is therefore not symmetric. The only distinction between the dispersed and the matrix phase is that latter is in excess concentration. Therefore, the MG model is best suited for low dispersed phase concentrations. On the other hand, the Bruggeman Approximation is symmetric for all the components of the medium and does not treat any of them differently[16]. The effective refractive index of the composite particles is

9

represented by 'n' and that of the dispersed phase and the medium are denoted by 'n1'and 'n2'respectively. The model is based on the volumetric comparison with f1 being the volume fraction of the dispersed phase in the composite system. The two models estimate the concentration of inorganic and organic phases in the hybridization process based on the required effective refractive index of the hybrid nanoparticles.
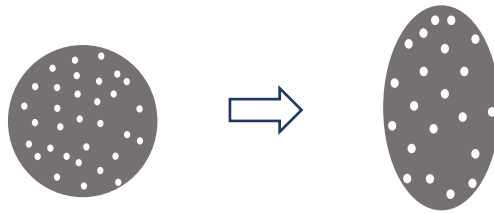
Fig. 1. 5: Structural modifications of the composite microparticles that can be oriented to form arrays.

The hybrid composition is favorable for emulating the moth-eye configuration as each phase has a specific function. The organic phase provides the skeletal framework to the resulting microparticles whereas the inorganic phase is used to impart functionality. These composite microparticles can then undergo structural modification via stretching to achieve the ellipsoid-like configuration (Fig.1.4). The hybrid morphology can be obtained by encapsulating the inorganic nanoparticles in a polymer matrix. Polymer encapsulation of inorganic nanoparticles is a process of forming a polymer shell around inorganic nanoparticles to achieve particles with a hybrid configuration. Various factors like surfactant concentration, monomer solubility, monomer concentration, pigment concentration, pH, temperature, and the role of initiator are responsible for influencing the outcome of the synthesis [17]. Janssen, R. Q. F. encapsulated TiO_2 nanoparticles using styrene and acrylate-based monomers and evaluated the role of process variables on

particle formation. The encapsulation was seen to be favorable when the polymer and the pigment were of comparable polarity. It is also conducive to have solvent polarity different from that of the other components because otherwise, the encapsulated particles may suffer from severe polymer desorption [17]. It is previously reported that the surfactant concentrations below the critical micelle concentration (CMC) give optimal encapsulation results. The CMC is the concentration above which the surfactant molecules aggregate to form clusters that usually have the polar hydrophilic ends pointing outwards and the non-polar amphiphilic forming the core. Additionally, surface modification/functionalization of the inorganic species improves the encapsulation efficiency as the nucleation of the monomer occurs preferentially at the interface of the inorganic-organic phase. Starve feeding the monomer i.e., the periodic introduction of the monomer or slow rate of monomer addition ($\approx<$ 1 ml/h) into the encapsulation process prevents homogenous nucleation of monomer molecules and enhances polymer dispersion in the solvent.

Haga et al. synthesized titania-polystyrene (PS), titania-polymethyl methacrylate (PMMA) composite microparticles using free-radical emulsion polymerization. Titania microparticles, water, and monomer are introduced into a four-necked flask equipped with a stirring apparatus, a condenser, and an N_2 introduction pipe, and after a required temperature controlling time, the encapsulating polymerization was started by adding the initiator into the flask. The initiator for polymerization is a free radical generating azo-compound namely 2,2'-azobis-(2-amidinopropane) dihydrochloride) (AAPH) used for synthesis at a basic pH and 4,4'-azobis (4-cyanovaleric acid Na-salt) (ACPA) for synthesis at a basic pH. The reaction slurry was then separated using organic solvents. Acetone was used to extract the TiO_2-PMMA microparticles whereas benzene was used in the case of

polystyrene synthesis. A 70% polymer conversion was reported with a 20% encapsulation efficiency. The encapsulation efficiency was evaluated by thermogravimetry analysis. Electrostatic interaction between the surface charge of the inorganic powder and the charge of the polymer chain end is critical for efficient encapsulation [18]. In addition, it was found that the polymerization reactions where the ends of the polymer chain and the metal oxide surface are oppositely charged give a better yield of encapsulated microparticles.

Roebuck et.al demonstrated a versatile method to encapsulate calcium carbonate ellipsoidal microparticles with a shell of methyl methacrylate (PMMA) polymer by conventional free-radical emulsion polymerization. The process was divided into two steps with the first being the encapsulation of inorganic particles with a primer layer followed by a shell thickening step using an acrylate polymer. Di(ethylene glycol) diacrylate (DEGDA) was used to form the primer layer on the inorganic microparticles. A difunctional monomer was desired to produce a fully cross-linked system so that the calcium carbonate core is kinetically trapped within the polymer shell and so that the composite material could potentially be processed since particles encapsulated in a non-cross-linked polymer shell exhibit dewetting when heated above the Tg of the said polymer [19]. However, the transmittance electron microscopy analysis showed large blobs of the polymer at the interaction sites suggesting dewetting of the polymer at the surface. The dewetting of DEDGA was minimized by the addition of methacrylic acid (MAA) monomer leading to a DEDGA/MAA primer mixture to promote the wetting of the calcite surface. The resulting encapsulated calcite microparticles were etched by adding 1 M HCL to form hollow ellipsoidal microparticles of DEDGA/MAA confirming the engulfment of the inorganic particles. The primer shell hollow particles were then thickened by adding methyl

methacrylate (MMA) monomer to the reaction mixture. Ammonium persulfate was used as the radical generating initiator for the polymerization of the MMA monomer. The presence of the primer layer facilitates efficient encapsulation with an efficiency of 100%. However, the encapsulated particles coagulate after formation which is evident in the microscopy images. There is a larger tendency of agglomeration for inorganic reactant constituents of particle size less than 100 μm. Moreover, the synthesis is carried out at an elevated temperature of 70 ⁰C which affects the economic feasibility of the process for scale-up. The size of the calcium carbonate-MMA composite particles was reported to be about a micron. A particle size ranging from 300-700 nm is desirable for anti-reflectivity. The smaller particles have a larger tendency of agglomeration as compared to micron-sized particles.

We employ a synthesis scheme at ambient temperature that involves a simple anionic polymerization. Here, synthesis does not require a primer coating material or an initiator for encapsulation. The reaction is performed in an aqueous medium where the polymerization is pH initiated.

1.3 Potential applications in cold spray applications

Although our principal objective is to create hybrid particles suitable for antireflective coatings, generally composite chemistries with tunable functionalities (dielectric, magnetic, optical) are of great interest for additive manufacturing coating technologies. Cold spray as well as other additive manufacturing technologies offer promise for rapid, efficient, and reproducible production of both film-based and 3-D device structures. In cold spray, the organic resin that forms the feedstock is accelerated through a supersonic gas jet of either helium or hydrogen at a speed up to 1200 m/s. Due to the high

impact, the resin undergoes plastic deformation and adheres to the surface. Organic polymer materials are central to these processes and the available platform of resins is wide but lacking in terms of many desirable applications including light (visible and IR), electromagnetic, and energy management as well as mechanical metamaterials. Typically, processed polymers require additional downstream modification steps to create functional materials or devices. Inorganic constituents with physicochemical properties that have applicability in the above fields can be embedded in the organic phase with an effort to develop composite metamaterials for coatings with tunable properties. Hybrid composites can be synthesized where the inorganic constituent can be varied as per the targeted functionality. The resulting metamaterials can then be used as a feedstock in techniques such as cold spraying for developing materials with desired properties.

1.4 Objectives

As described above, there is tremendous interest in creating particles with a hybrid configuration for the development of novel materials. It is thus worthwhile to develop a versatile strategy for incorporating inorganic nanoparticles into an organic matrix and study the effects of several process variables on their formation. The goal of this thesis is to develop a robust strategy for synthesizing TiO_2-DEMM microparticles and control the inorganic incorporation in them. We first present the results of a four-factor design of experiments which elucidates the critical process parameters to forming hybrid particles. We then use the optimal synthetic procedure to demonstrate how the incorporation of inorganic nanoparticles can be controlled over a wide weight fraction, and identify the inorganic surface chemistry as an important parameter to control the final particle colloidal stability. Lastly, to illustrate the versatility of the approach different inorganic constituents

(CdTe, ZnO) are successfully incorporated and preliminary nanoimprint lithography experiments are performed.

CHAPTER 2

Materials and Methods

2.1 Synthetic Procedure

As we have seen from the literature, free radical emulsion polymer is predominantly used for the synthesis of composite microparticles. However, this research work employs the use of a novel malonate monomer with excellent coating properties, that undergoes anionic polymerization[20].

2.1.1 Anionic polymerization

1.	TiO₂ concentration	1 wt% per solvent
2.	Surfactant concentration	9mM
3.	DEMM (m/i ratio)	4.255
4.	Water	10 ml
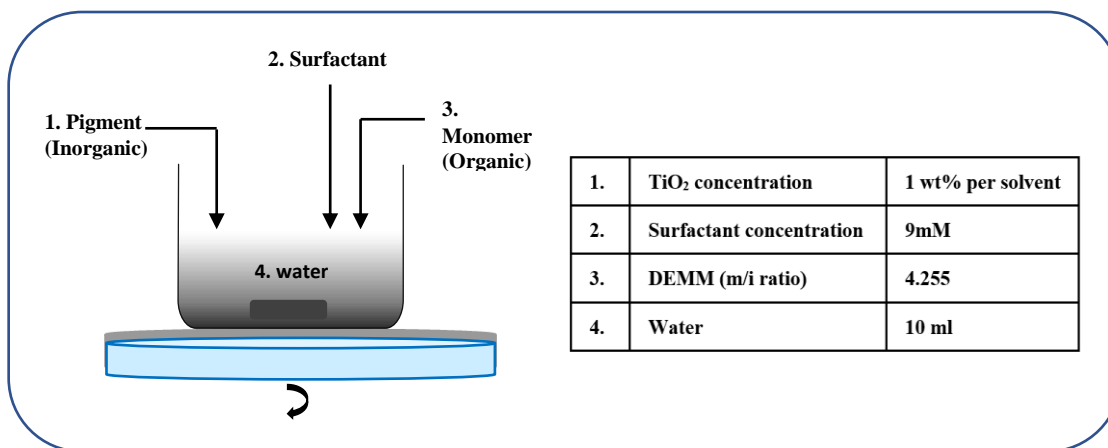
Fig. 2. 1: Anionic polymerization for hybrid particle synthesis

Anionic polymerization is a type of chain-growth polymerization also known as addition polymerization that consists of the polymerization of monomers initiated with an anionic group. Anionic polymerization involves living polymerizations, where the chain termination reactions can be suppressed. This allows control of the structure and composition of the resulting polymeric chains. In anionic polymerization, a monomer polymerizes upon reacting with an initiator and generates a carbanion center. The active site propagates and grows along the polymer strand with the addition of more monomers

until it is deliberately terminated by a terminator. Anionic polymerization is a well-established technique used to synthesize a wide variety of polymers. For example, block copolymers, such as poly(styrene−butadiene) are industrially important thermoplastic elastomers synthesized using anionic polymerization [20]. Telechelic polymers synthesized via anionic polymerization are important building blocks for polymer architectures, such as star, hyperbranched, and dendritic polymers. One challenging aspect of the anionic polymerization process is maintaining the reactivity of the chain ends. Moisture, oxygen, carbon dioxide, and other contaminants in the reaction environment can terminate the reaction prematurely.

We modify the anionic polymerization reaction by adding an inorganic pigment (titania nanoparticles) before initiating polymerization (Fig. 2.1). The synthesis is conducted in the aqueous medium wherein we first add TiO_2 nanoparticles to 10 ml water. After several minutes of stirring, we add an anionic surfactant, sodium dodecyl sulfate (SDS) to the titania in the water solution. The surfactant acts as a colloidal stabilizer by inducing charge at the titania surface. A stronger surface charge leads to a preferential monomer polymerization at the surface sites. Additionally, the presence of charge of contrasting polarity between the inorganic surface and the active site in the monomer results in better encapsulation of the inorganic nanoparticles. The surfactant concentration is set to lower or equal to the critical micelle concentration (CMC) value. Hybrid particles from synthesis at surfactant concentration higher than the CMC value result in agglomeration. This is caused due to formation of micelles that entrap monomer molecules in their nonpolar core which results in secondary nucleation leading to agglomeration. For reactions in acidic conditions, we modify the pH using hydrochloric acid (HCl). The

synthesis is run at two pH values, 4.5 and 7. Finally, after the pH adjustment, we introduce the monomer (diethyl methylene malonate) at a starved fed rate of 1 ml/h. The slow rate of addition minimizes the secondary nucleation of the monomer in the solution [17]. Also, starved fed monomer addition minimizes homogenous nucleation and promotes heterogeneous nucleation. Heterogenous nucleation refers to the new phase formation on a site at an interface whereas homogenous nucleation refers to that in the bulk. The reaction is run for 4 hours at room temperature at 600 rpm. The synthesis is stopped by turning off the magnetic stirrer and the solution is transferred to a dialysis tubing for separating the undesirable constituents. The polymer particles separated from the unreacted constituents are then used as a sample for analysis.
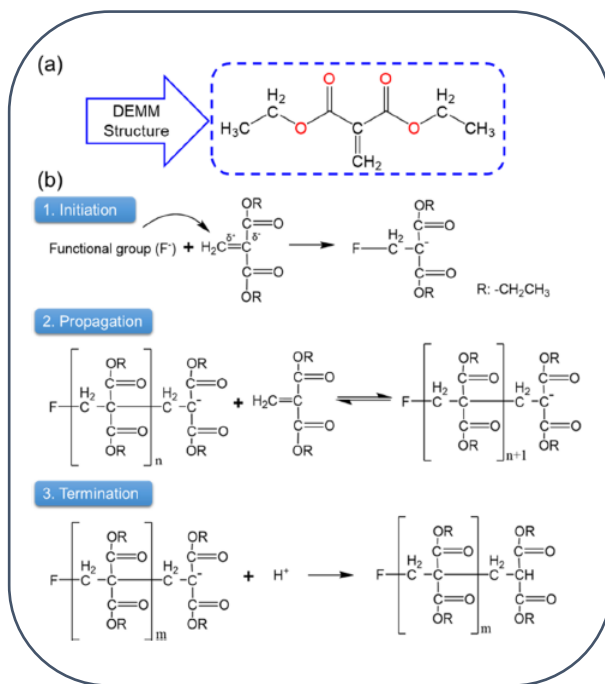

Fig. 2. 2: Diethyl methylidene malonate, (a) chemical structure (b) polymerization mechanism. [20]

The organic constituent of the reaction, diethyl methylene malonate (DEMM) is a novel monomer. Diethyl methylene malonate (Chemilian M1000, DEMM) and were

provided by Sirrus Inc. (Loveland, OH). Fig. 2.2 displays the structure of DEMM, which consists of two electronegative ester groups that lead to an imbalance in the distribution of electrons on the molecule. Negative charges get delocalized onto two ester groups, which result in the electro positivity of the vinyl groups. Thus, the vinyl group provides a site where anionic functional groups could easily attack to form an active center, enabling the anionic polymerization of DEMM. The polymerization scheme is shown in Figure 2.2b which indicates the initiation of DEMM by anionic functional groups, the elongation of the polymer chain, and the termination of reaction by a strong acid. Hydroxide ions (OH−) in water could initiate DEMM, and our study demonstrates that DEMM could polymerize in water at a pH value of 4 or greater without adding any additional initiators. The potential mechanism of polymerization is validated by the NMR analysis, which displays the consumption of a double bond with a more than 99.9% conversion rate. Huang et.al conducted experiments of anionic polymerization at varying pH (Fig. 2.3). Visually, the production of an emulsion occurred at pH values lower than 6. At pH values of 6 and 7, white cotton-like polymer separated from the emulsion, which indicated the formation of a higher-molecular-weight (MW) polymer (Figure 2.3b). The correlation between the pH value and the molecular weight of the polymer was verified using Size exclusion chromatography. The molecular weight was reported to increase with increasing pH. The polymerization of DEMM in water synergistically results from both the initiation by OH− and termination by proton. The hydroxyl group (OH−) in water play the role of the anionic

19

initiator, while protonic hydrogen ions (H+) act as the terminator to stop the polymerization. At acidic conditions, termination plays a more dominant effect, leading to low molecular weight polymer particles. Higher pH values are associated with lower levels of H+, so the chain continues to propagate (and less termination occurs), leading to a high-MW poly (DEMM). [20]
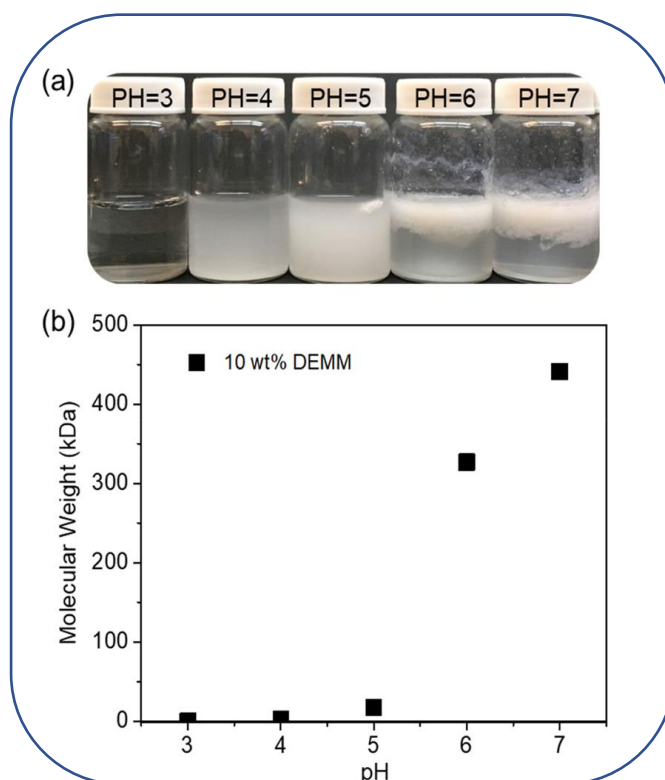
Fig. 2. 3: (a) Influence of pH of the solution on the polymerization of DEMM (b) Variation of the molecular weight of poly(DEMM) as a function of the pH of the solution.[20]

2.1.2 Inorganic constituents

As mentioned above we use titania (TiO$_2$) nanoparticles in the synthesis scheme as the inorganic part and diethyl methylene malonate (DEMM) as the organic part. We use sodium dodecyl sulfate (SDS) an anionic surfactant to uniformly disperse the TiO$_2$

nanoparticles and initiate polymerization at the particle surface. These three reactants form the major constituents of the synthesis scheme. In addition, TiO_2 functionalized with polyacrylic acid, CdTe quantum dots, and ZnO nanoparticles have also been used as the inorganic constituent.

The TiO_2 nanoparticles have a particle size of 30 nm with no surface functionalization. The bare titania particles are obtained from US Research Nanomaterials, Inc. Titanium dioxide is the most widely used white pigment because of its brightness and very high refractive index. Titanium dioxide crystal size is ideally around 220 nm (measured by electron microscope) to optimize the maximum reflection of visible light. However, abnormal grain growth is often observed in titanium dioxide, particularly in its rutile phase. The occurrence of abnormal grain growth brings about a deviation of a small number of crystallites from the mean crystal size and modifies the physical behavior of TiO_2. The optical properties of the finished pigment are highly sensitive to purity. As little as a few parts per million (ppm) of certain metals (Cr, V, Cu, Fe, Nb) can disturb the crystal lattice so much that the effect can be detected in quality control. TiO_2 is also an effective opacifier in powder form, where it is employed as a pigment to provide whiteness and opacity to products such as paints, coatings, plastics, papers, inks, foods, medicines (i.e., pills and tablets), and most toothpaste. Opacity is improved by optimal sizing of the titanium dioxide particles. These optical properties can be exploited to develop composite particles that have a higher refractive index and modifiable geometry.

Cadmium telluride is a stable crystalline compound majorly used for building photovoltaics in semiconductor applications. The nanostructured quantum dots are surface modified with 3 mercaptopropionic acid (3-MPA). 3-Mercaptopropionic acid (3-MPA) is

an organosulfur compound with the formula $C_3H_6O_2S$. It is a bifunctional molecule, containing both carboxylic acid and thiol groups. The surface modification with 3-MPA results in a negative surface charge due to the dissociation of the acidic group.

2.2 Design of Experiments

The process variables associated with the anionic polymerization affect the formation of the particles of composite organic-inorganic morphology. From literature, factors such as the inorganic concentration, organic to inorganic ratio, type of surfactant, the concentration of the surfactant, type of initiator, initiator concentration, monomer addition rate, reaction temperature, and the pH of the solution influence the particle size and microstructure, presenting a potentially large experimental parameter space. By analyzing the literature and in particular how it relates to the polymerization of DEMM, we can identify the potentially most important variables for study. The emulsion polymerization for polystyrene (PS)-TiO_2 and poly (methyl methacrylate) (PMMA)-TiO_2 hybrid particles reported that the surfactant concentration should be just under the critical micelle concentration (CMC) to prevent coagulation of the emulsion to have the best encapsulation results [17]. The titania nanoparticles show a strong degree of agglomeration due to low surface charge and particle size (30 nm). A pigment (TiO_2) concentration from 0.1 to 10 wt% is generally employed for the synthesis of composite particles to minimize the agglomeration of inorganic nanoparticles. The organic to inorganic ratio is critical as a high monomer to inorganic ratio may result in polymer desorption from pigment surface post-synthesis or cause free polymer formation [17]. The glass transition temperature for poly (DEMM) is reported to be ranging from 25 ⁰C to 40 ⁰C [21]. Therefore, we carry the reaction at an ambient temperature of 25 ⁰C. From Huang. et. al work discussed in the previous section the desirable range of pH for synthesis is from 4 to 7.

In order to systematically study the role of each factor in the synthesis of TiO_2-DEMM particles, we design experiments such that we can study the individual as well as

the interactive effects of each process variable. We employ a Box-Behnken design also known as BBD design, wherein each factor participating in the design is set to a high and low value. We have a total of four factors, namely the inorganic concentration, surfactant concentration, monomer to pigment ratio, and pH of the solution. Each factor is set to two levels (low and high) leading to 16 combinations in the design (Table 2.1). The low and the high values are determined by referring to the published literature on the synthesis of composite microparticles. The particle size is measured by dynamic light scattering (DLS) for each experiment and the qualitative evaluation of the inorganic incorporation is performed by scanning electron microscopy (SEM).

Experiment Number	TiO$_2$ concentration (wt% per solvent)	g monomer/g TiO$_2$	pH	Surfactant concentration (mM)
1	1	4.255	7.2	9
2	1	4.255	7.2	6
3	1	4.255	4.5	9
4	1	4.255	4.5	6
5	1	1.5	7.2	9
6	1	1.5	7.2	6
7	1	1.5	4.5	9
8	1	1.5	4.5	6
9	0.5	8.51	7.2	9
10	0.5	8.51	7.2	6
11	0.5	8.51	4.5	9
12	0.5	8.51	4.5	6
13	0.5	3	7.2	9
14	0.5	3	7.2	6
15	0.5	3	4.5	9
16	0.5	3	4.5	6

Table 2.1: Box Behnken design of experiments

2.3 Particle Characterization

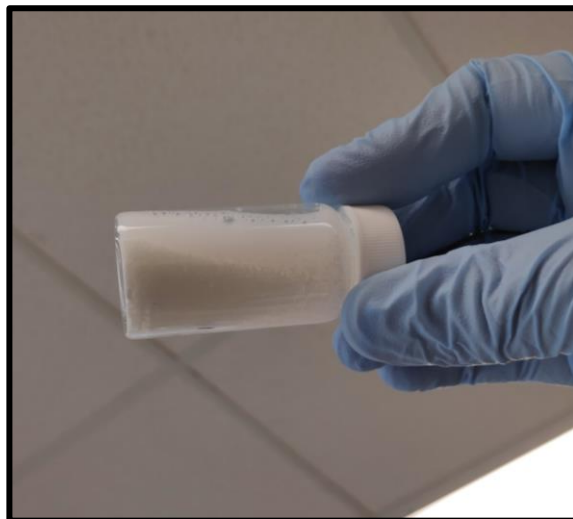On completion of the synthesis, the hybrid particles are seen to precipitate out of the solution (as shown below).

Fig. 2. 4: Composite TiO$_2$-DEMM microparticle precipitation

The solution is then transferred to a laboratory dialysis tubing and placed in a 1 liter, 9mM SDS solution for dialysis. The dialysis helps separate the unreacted monomer and titania particles and is conducted over three days by replacing the SDS solution daily. The sample is transferred to the 20 ml vial followed by three dilutions (solvent exchange) with 9mM SDS to further separate the unreacted constituents. 100 or 200 microliters of the sample are diluted in 10 ml SDS solution for Light microscopy analysis. We use Nikon Ti2- Eclipse inverted microscope for bright-field and fluorescence imaging. The microparticles are diluted (10 μl in 10 ml) 0.1 mM KCl solution for Dynamic Light Scattering Analysis. The equivalent dilution criterion is used for zeta potential measurements. Malvern Zetasizer Nano is used for particle size and zeta potential measurements. The composite particle suspension is diluted (50 μl, 100 μl, 1000 μl sample

in 10 ml SDS solution) in a 20 ml pyrex vial for Scanning Electron Microscopy analysis. The samples were mounted on a silicon wafer attached to an SEM stub and placed in a desiccator for drying. The dried sample was then sputter-coated with a thin film of gold (Au) to enhance the electron excitation and image quality. TA instruments Q50 model is used for thermogravimetry analysis. The sample post-dialysis is transferred to a 20 ml vial and the supernatant is decanted. The settled mass is then dried in a vacuum oven at 60 ºC. The dried mass is then transferred to the platinum pan for TGA analysis. The qualitative and the quantitative results are discussed in the following section.

CHAPTER 3

Results and Discussion

3.1 Hybrid DEMM/TiO₂ microparticles

We first present results of the design of experiments performed to generate hybrid TiO_2-DEMM microparticles. The hybrid inorganic-organic microparticles were characterized by measuring particle size and observing the degree of inorganic incorporation via SEM.

3.1.1 Controlling particle size

Particle size measurement was conducted for each of the 16 experiments that constituted the BBD design. Each experiment formed one combination of factors at a high or a low level. Interestingly, we observed a consistent pattern of a decrease in particle size
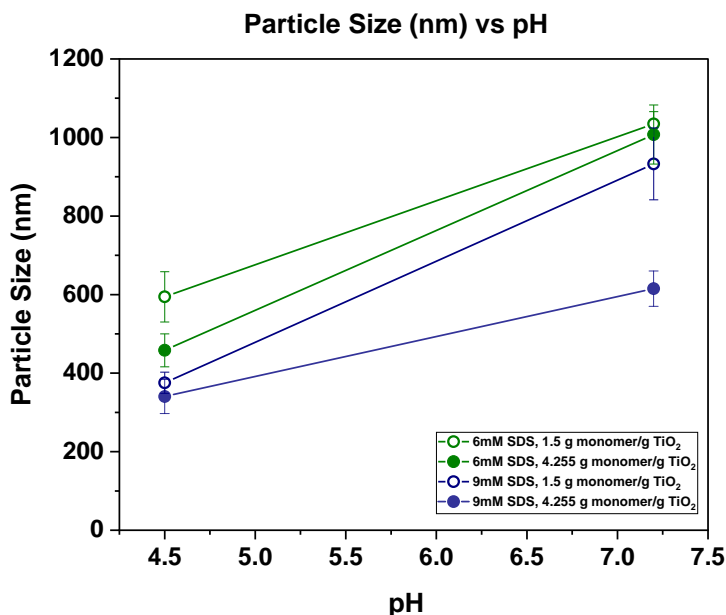

Fig. 3. 1: Particle size (nm) of the composite microparticles vs pH of the reaction solution for experiments where the surfactant conc. and the monomer to inorganic (m/i) ratio are both at low level (green hollow data points); low surfactant conc., high m/i ratio (green solid); high surfactant conc., low m/i ratio (blue hollow); high surfactant conc.; high m/i ratio (blue solid)

as a function of the pH and the surfactant concentration from the first eight experiments in the table mentioned above (Table. 2.1). The latter eight experiments were majorly identical to the former eight experiments except for the initial inorganic concentration (Table 2.1). However, there was no significant correlation between the latter eight experiments.

For the experiments where the surfactant concentration and the monomer to inorganic ratio were at a low level, we measured particle size of about 520-680 nm for a pH of 4.5 and about a micron (1000 nm) for a pH of 7.2 (Fig. 3.1). The particle size decreased at both the pH values for the case where the monomer to inorganic ratio was set to the high level while keeping the surfactant concentration to the lower level. We recorded an even further decrease in the particle size for the experiment where the surfactant concentration was set to the high level keeping the monomer to inorganic ratio to the lower limit. Finally, for the case where both the factors were set to a high level, we recorded the least particle size, ranging from 300-350 nm for a pH of 4.5 and 550-600 nm for a pH of 7.2. It can be inferred from these results that the pH and the surfactant concentration had the most dominant role in influencing the particle size of the resulting composite TiO_2-DEMM microparticles. The individual effects of factors participating in the design influenced the particle size more than the interactive effects of multiple factors. The lower pH corresponds to a higher concentration of H^+ ions that are responsible for the chain termination of poly (DEMM). The presence of an acidic environment results in polymer chains of lower molecular weight, reported by Huang. et.al and thus lower particle size, confirmed by these results. Another potential reason for the reduction of particle size at a lower pH is the difference in polarity between the inorganic surface and the solvent. This

minimizes aggregation between the inorganic particles which leads to a reduction in the particle size.

Control experiments were also performed without inorganic constituents and reaction conditions corresponding to the smallest particle size measured from the design of experiments (pH 4.5, 9mM SDS). From DLS, the particle size of DEMM nanoparticles without the inorganic pigment from this optimal synthetic scheme is between 200 to 250 nm. This indicates a lower bound on the particle size and is indirect evidence of the successful incorporation of inorganic nanoparticles causing the final particle size to increase.
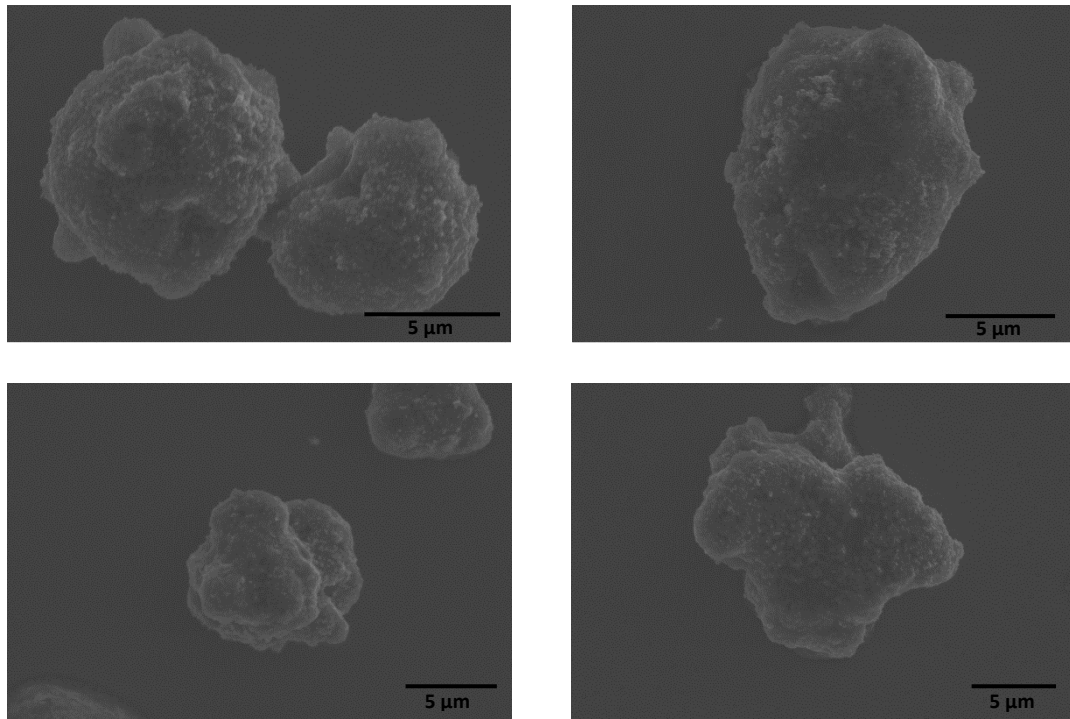

Fig. 3. 2: SEM images of hybrid TiO$_2$-DEMM microparticles. Titania nanoparticles can be seen inside the globules of the polymer matrix.

3.1.2 Importance of surface functionalization on colloidal stability

The experiments that give us the particle size in the lower range were imaged using SEM. The images of the microparticles revealed the incorporation of the inorganic phase in the organic matrix. A uniformly distributed white dot-like nanoparticles can be seen embedded in the organic phase (see Fig.3.2).
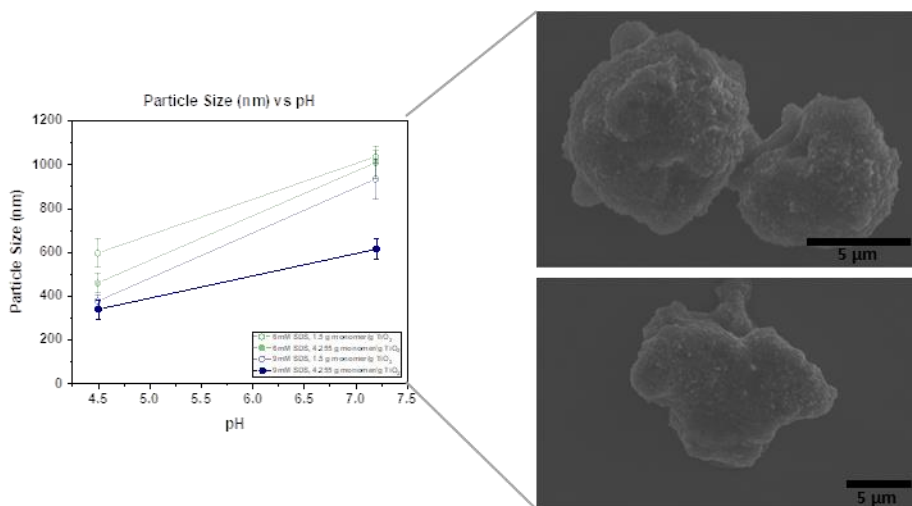

Fig. 3. 3: Disparity between the particle size measurement from light scattering analysis (350-600 nm) to that from SEM images (5-10 μm)

However, the particle size measured from the SEM image analysis is not consistent with light scattering particle size measurement. We obtain a particle size of 5-10 micrometers from the image analysis as opposed to 350-600 nm from DLS (Fig.3.3). This inconsistency in particle size is majorly attributed to the tendency of the particles to agglomerate with time and as the solution dries on the SEM stub. The colloidal stability of the emulsion post-synthesis reduces with time due to the absence of a stronger surface charge between the hybrid particles. Moreover, the effect of the gravitational field leads to sedimentation which promotes the formation of agglomerates. An immediate solution to

overcome the agglomeration of these hybrid microparticles is to develop a stable colloidal solution.

To achieve that we synthesize hybrid microparticles by having the inorganic phase be titania (TiO_2) nanoparticles capped with polyacrylic acid (PA). The PA results in a surface charge of -50 mV in comparison to a lower surface charge in the case of bare titania nanoparticles. A higher magnitude in surface charge results in better colloidal stability and lower aggregation. The particle size measurement by DLS and SEM for polyacrylic acid capped titania hybrid particles (PA-TiO_2-DEMM) were in a better congruence in comparison to those with bare titania (see Fig. 3.4). The incorporation of inorganic PA-TiO_2 nanoparticles can be visually seen from the SEM images.

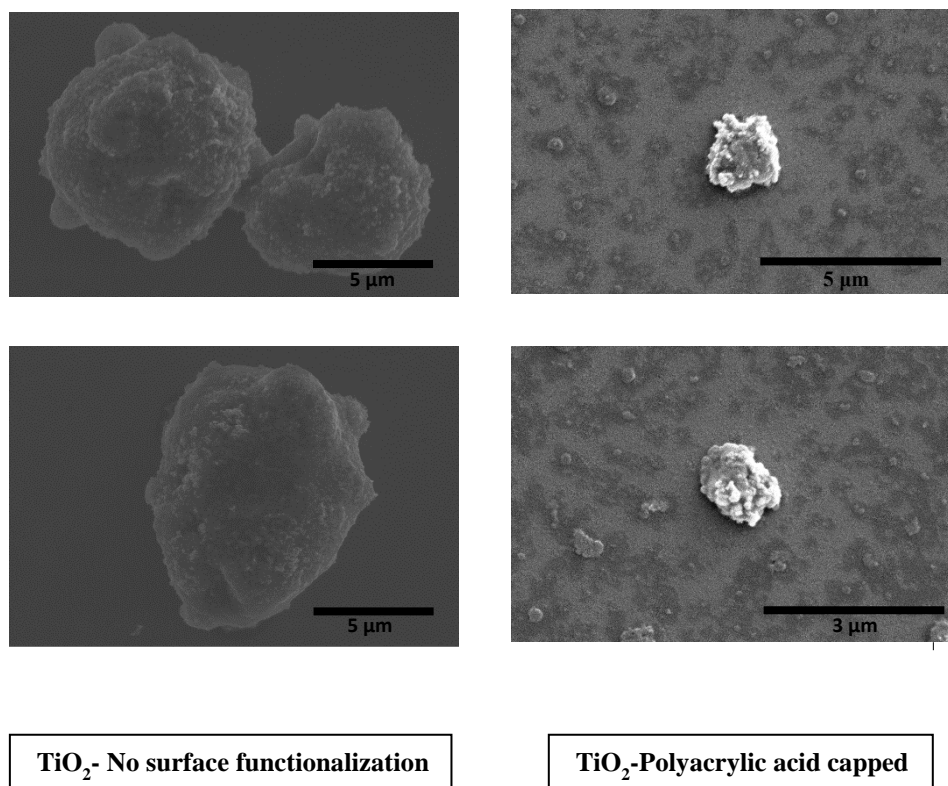| **TiO_2- No surface functionalization** | **TiO_2-Polyacrylic acid capped** |

Fig. 3. 4: Particle size difference between hybrid microparticles from bare titania nanoparticles (5 μm-10 μm) and PA-TiO_2 nanoparticles (700-1200 μm)

3.1.3 Controlling inorganic loading

The next objective of this research work is to control the incorporation of the inorganic titania nanoparticles in the organic phase. To investigate that we synthesized hybrid TiO_2-DEMM microparticles for varying inorganic concentrations. The range of inorganic concentration varied from 0.1 wt % per solvent to 5 wt% per solvent. The synthesis product was then transferred to a dialysis tubing for dialysis. For each synthesis sample, a parameter called the "expected weight fraction" was evaluated. This value illustrates the case where all the titania is incorporated in the organic phase. The expected weight fraction value is evaluated as follows:

$$Expected\ wt.\ fraction = \frac{g\ TiO_2\ added}{g\ TiO_2\ added + g\ polymer\ added}$$

The supernatant from the dialysis was decanted and the settled mass was dried in a vacuum oven at 60 °C. A white sticky solid mass was obtained which was used as a sample for Thermogravimetry Analysis (TGA) analysis to quantify the inorganic incorporation. TGA is an analytical technique used to evaluate a constituent's thermal stability and its fraction of volatile components by estimating the weight change that occurs as a function of temperature. Diethyl methylene malonate polymer has a boiling point ranging from 250-300 °C. The titania has a boiling point above 1000 °C. We load our sample on a platinum TGA pan and input a ramp gradient in temperature from 25 C to 500 C at a rate of 25 C/min. We observe a sudden decrease in weight percent after passing the expected DEMM boiling point, as shown in Fig 3.5.
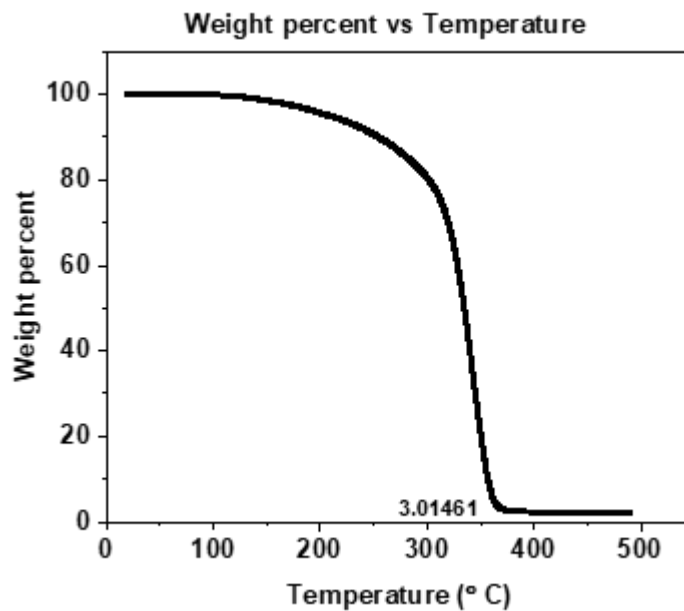
Fig. 3. 5: Weight percent vs Temperature (C) for composite microparticles from TGA analysis.

We observe a similar trend of weight percent reduction at around 300 °C for samples with varying inorganic concentrations. We evaluate the weight fraction of the residue titania from the TGA analysis for all the samples. These values are termed as the obtained weight fraction titania from the synthesis. To better understand the influence of inorganic concentration on its incorporation, we compare the obtained weight fraction with the expected weight fraction as shown below.
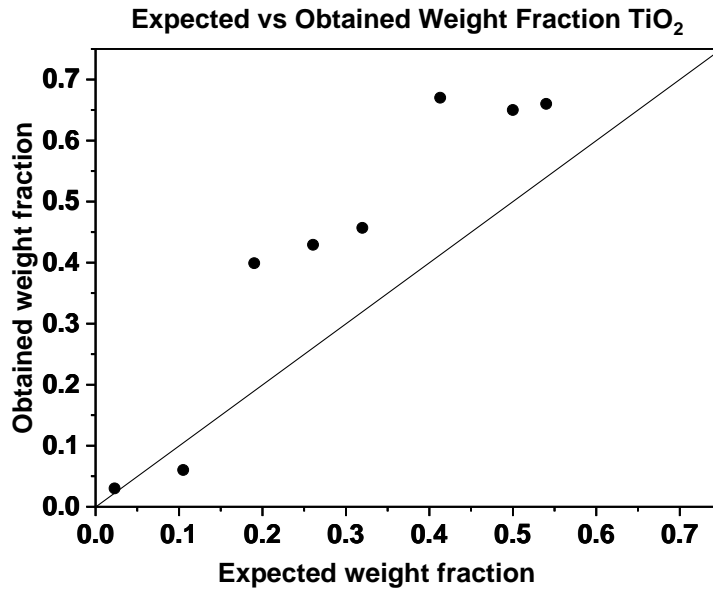
Fig. 3. 6: Obtained weight fraction vs Expected weight fraction for TiO$_2$-DEMM hybrid particles

For increasing titania concentration in the synthesis reaction, we record a higher amount of titania incorporation in the composite particles, as expected. The effective refractive index from the two models discussed above indicates a RI ranging from 1.45 to 1.7. The straight line in Fig.3.6 represents the scenario where all the titania would be incorporated in the polymeric phase resulting in the expected weight fraction being equivalent to the obtained weight fraction. These calculations were done assuming complete conversion of the DEMM monomer. Most of the data points fall on the upper side of this representative line indicating the presence of an unreacted monomer in the synthesis reaction. The polymer conversion increases with increasing titania concentration as the data points show a similar trend in comparison to the representative line. From calculations, roughly 80 % monomer is converted to polymer for data points with expected weight fraction above 0.25.

The success of the encapsulation process is estimated by the encapsulation efficiency which is defined as the amount of surface polymer per amount of monomer added to the reaction mixture and the polymer content which can be defined as the amount of polymer at the pigment surface per amount of encapsulated pigment. The polymer content can also be defined with respect to the amount of bare pigment without encapsulation.

$$Polymer\ Content\ (P.C) = \frac{w - w_0}{100}$$

where,

w = loss in weight (polymer + titanate + crystal water) of the encapsulated pigment determined by thermogravimetric analysis. (wt%)

w_0 = loss in weight (titanate + crystal water) of the modified pigment by thermogravimetric analysis. (wt%)

$$Encapsulation\ efficiency\ (\eta) = \frac{P.C * p}{m} * 100(\%)$$

where,

p = total amount of modified pigment added during the reaction (g)

m = total amount of monomer added during the reaction (g)

Sample number	Inorganic Concentration (wt%) per solvent	P.C	Encapsulation Efficiency (η)
1	0.1	0.97	2.28
2	0.5	0.94	11.05
3	1	0.6	14.10
4	1.5	0.58	20.45
5	2	0.56	26.32
6	3	0.31	21.86
7	4.25	0.33	33
8	5	0.31	36.43

Table 3.1: Polymer content (P.C) and Encapsulation Efficiency (η) of TiO_2

We are able to achieve a polymer content ranging from 0.31-0.97 with an encapsulation efficiency from 2-36 %. The average encapsulation efficiency is 20.68 %

3.1.4 Optimal synthesis scheme

The optimal synthetic process is determined by evaluating the experiments that give the least particle size from the design of experiments. This is crucial because the light interacts with patterned surfaces of sub-wavelength particles differently than particles with dimensions greater than the wavelength. For this reason, it is desirable to synthesize composite particles with dimensions less than 400 nm.

From the electron microscopy, we confirm the formation of particles with a hybrid configuration from our synthesis scheme. We validate the effects of process variables, pH, SDS concentration, TiO_2 weight fraction, on the particle size from a simple design of experiments. We also monitor the titania incorporation by tuning its concentration in the polymerization reaction. Based on these initial results the optimal synthetic procedure for developing hybrid microparticles from other inorganic constituents is identified. In order to produce ~400 nm particles, the reaction pH is 4.5, the surfactant concentration is 9mM and the inorganic concentration is set to 1 wt%. The amount of monomer added to the reaction is approximately four times (4.255) the inorganic by weight.

3.2 Extension to other inorganic constituents

The optimal synthesis scheme was first employed using cadmium telluride quantum dots. The ~10 nm diameter cadmium telluride nanoparticles were synthesized by the Kittilstved Lab and are suspended in water at a concentration of 10 wt%. All the process variables and reaction constituents are identical. The titania nanoparticles are replaced by the CdTe quantum dots with all other process parameters remaining constant. Post synthesis we obtain similar precipitation of particles as observed in titania synthesis. The CdTe-DEMM composite particles however have a lower polydispersity index and form a homogenous suspension, owing to the higher surface charge and better colloidal stability (Fig. 3.7).
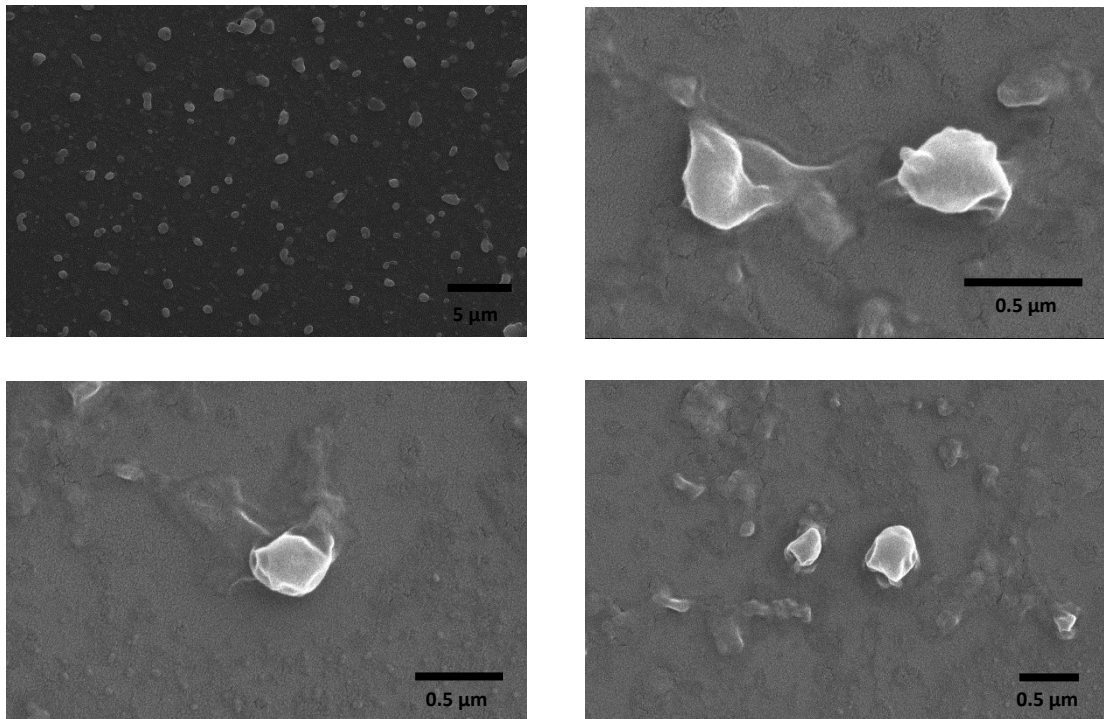

Fig. 3. 7: SEM images of CdTe-DEMM hybrid particles showing a homogenous distribution.

The incorporation of the CdTe nanoparticles is difficult to validate from the SEM images. However, CdTe nanoparticles are fluorescent and have an excitation wavelength of 365 nm and an emission wavelength of 700 nm. Fluorescence microscopy is used to investigate whether the CdTe nanoparticles are incorporated in the organic matrix, and as expected the hybrid microparticles are fluorescent, confirming the presence of CdTe nanoparticles in the composite. (Fig. 3.8)
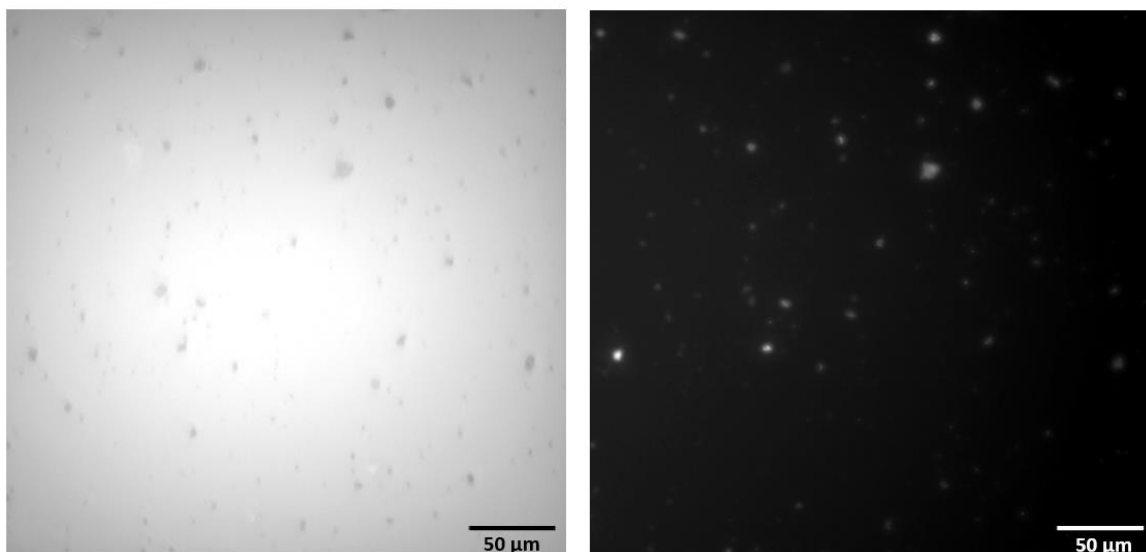

Fig. 3. 8: Bright-field (left) and fluorescence image (right) of CdTe hybrid microparticles..

In addition, we used the identical synthetic scheme for zinc oxide (ZnO) nanoparticles. The particle size of the ZnO particles was estimated to be ~ 6 nm These nanoparticles were capped with l-arginine that led to a positively charged surface due to the delocalization of the protonic charge from one nitrogen molecule to another. We were able to synthesize hybrid ZnO-DEMM microparticles using an identical synthesis scheme as used before for previous inorganic constituents. However, the size of the composite particles was higher than the ones obtained from titania and cadmium telluride nanoparticles. This was confirmed with SEM imaging as shown below in Fig.3.9. The

ligand system at the ZnO surface has a weak surface charge evaluated from light scattering analysis. The ligand system with a weak electro-negative can be modified to a system with a higher magnitude of surface charge.
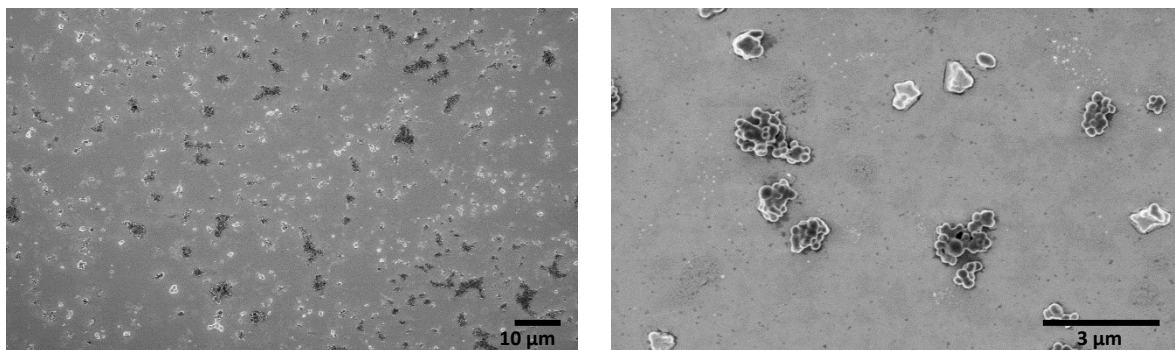

Fig. 3. 9: Aggregation of ZnO-DEMM hybrid microparticles from SEM imaging

When we analyze the particle size measurement from DLS, SEM and zeta potential measurements on the hybrid microparticles, an apparent correlation between inorganic nanoparticle functionality and hybrid particle stability is revealed. The DLS particle size is lower for inorganic constituents that have a higher magnitude in zeta potential, and SEM imaging of those samples indicated less agglomeration upon drying. Polyacrylic acid capped titania-DEMM and 3 MPA capped CdTe-DEMM have a zeta potential of about -30 mV and -40 mV respectively. These hybrid microparticles have a lower size than hybrid particles with other inorganic constituents (Fig. 3.10). Therefore, a general design principle to incorporating additional inorganic nanoparticles in this synthesis scheme is that a higher inorganic anionic surface charge results in improved colloidal stability which in turn leads to a lower aggregation and thus a lower particle size.
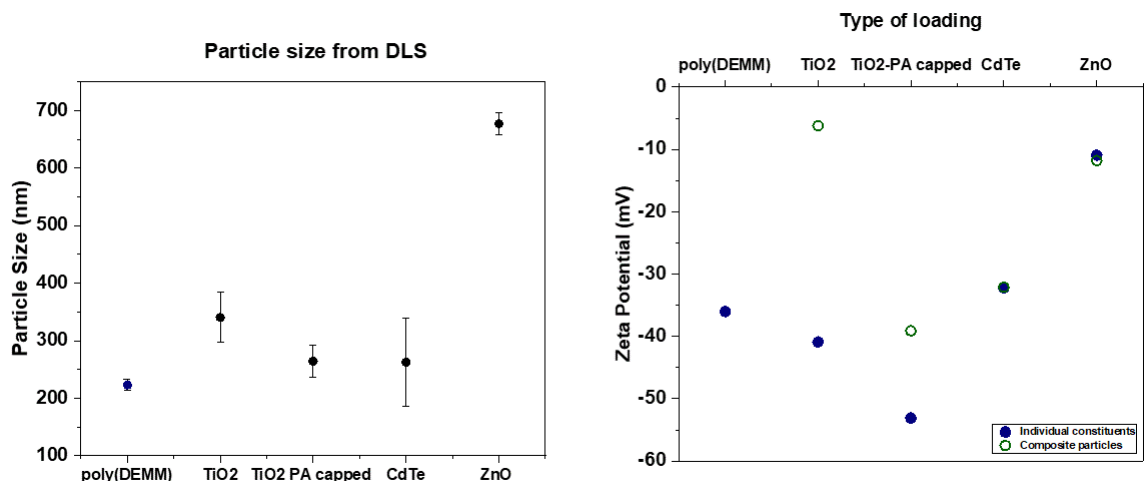
Fig. 3. 10: Comparison between the particle size and zeta potential of composite particles with different inorganic loading

In addition, zeta potential measurement also reveals the presence of inorganic nanoparticles at the hybrid particle surface, influencing the overall particle charge. Fig 3.11 shows the zeta potential of the inorganic nanoparticles suspended in water compared to the final zeta potential of the composite particles. We observe a change in zeta potential post-synthesis that confirms a surface modification of inorganic nanoparticles during synthesis.

A consistent result from these measurements is that the zeta potential is reported to decrease for hybrid particles in comparison to their inorganic constituents. This can be a major factor contributing to their agglomeration. The PA capped TiO_2 have the highest magnitude of zeta potential which resonates with the observation of a better colloidal stability post-synthesis. We are at least able to validate the formation of a new surface in the solution owing to the change in the zeta potential value. The zeta potential of bare poly (DEMM) microparticles is reported to be about -30 mV. The interaction of the two phases (inorganic-organic) lowers the zeta potential of the composite particles leading to their aggregation.
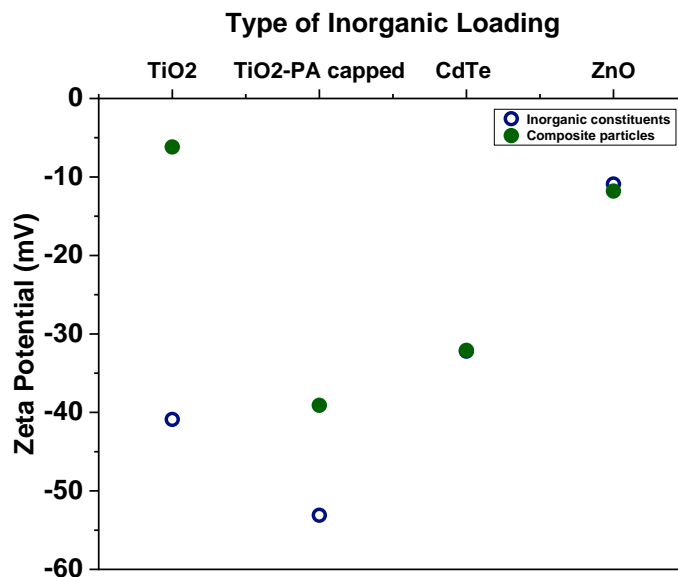
41

Fig. 3. 11: Zeta potential pre-synthesis (left) vs post synthesis (right)

3.3 Preliminary cold-spray experiments:
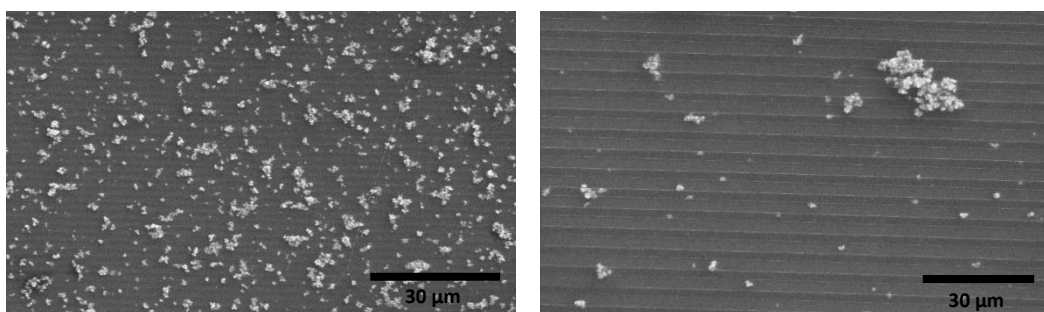
Fig. 3. 12: SEM images of the TiO$_2$-DEMM microparticles spin-coated on a silicon substrate

The TiO$_2$-DEMM sample is mixed with a 10 wt% solution of Polyvinyl alcohol (PVA) (Mowiol 4-88) in water (*courtesy of Watkin's Lab*). The resulting solution shows good mixing with no phase separation. However, it is difficult to determine its homogeneity due to the high opacity of the solution. The composite particle in PVA solution is then

spin-coated onto Si wafer at 2000 rpm, with an acceleration of 1500 rpm/s for 20 seconds to achieve a semifluid film. A 500 nm height, 500 nm width, 1 um pitch line patterned Polydimethylsiloxane (PDMS) stamp was placed on top, pressed onto the surface, and heated to 100ºC on a hot plate for 10 minutes. The stamp was removed to reveal the structure. The macroscopic appearance is hazy and has some optical diffraction from the structure, but the optical effect is faint.

It appears the matrix (PVA) and particles do not mix effectively, and that the aggregation prevents proper filling of the stamp. The PVA conforms to the stamp template but is not filled due to the contact issues between the stamp and imprint material. An alternate ligand system may be helpful for better coating results. A PEG silane capping agent (Kittlistved's Lab) can be a suitable modification as it keeps the particles dispersed and homogenous under high concentration.

CHAPTER 4

Conclusion and Future work

A successful demonstration of synthesizing composite inorganic-organic DEMM microparticles has been demonstrated. The composite particles are characterized qualitatively using SEM, and quantitatively using DLS and TGA. The hybrid microparticles were formed by modifying anionic polymerization to encapsulate titania and other inorganic nanoparticles by a novel monomer polyester chemistry. The particle composition and configuration are controlled by tailoring the synthesis variables.

This is achieved by systematically studying the influence of each process variable on particle formation using a formal design of experiments. Particles formed from the polymerization reaction are found to be predominantly affected by the surfactant concentration and the pH of the solution. Next, the inorganic incorporation of titania in the hybrid composition is evaluated at varying synthesis concentrations to develop strategies for controlling the functionality of the composite particles. A wide range of inorganic nanoparticle incorporation was achieved, although the results indicate the presence of unreacted monomers at higher pigment concentrations. The optimal synthetic scheme from the TiO_2-DEMM reaction is applied to other inorganic constituents to evaluate their capability to form hybrid particles. Additionally, a correlation between the particle size and its surface charge is reported to indicate the importance of forming stable colloids of composite particles using ligands on the inorganic nanoparticles.

Further work involves the characterization of the composite particles with compound detection techniques such as SEM-EDX. From the initial results, a persistent difficulty of agglomeration is observed between the composite microparticles upon drying

for electron microscopy. It is important to develop strategies for minimizing aggregation and form a stable colloidal suspension of composite microparticles for use in additive manufacturing applications. A potential solution is to generate a higher magnitude of contrasting polarity between the inorganic particle surface and the solvent during synthesis.

The hybrid particles are constructed to form a feedstock that can be transformed into thin films using traditional coating techniques. It is therefore important to investigate the coating properties of the hybrid microparticles. Also, the elastic properties of the microparticles can be evaluated to estimate their feasibility for structural modifications. Anisotropic particles can be formed by applying mechanical stress. [22]

Moreover, it is also crucial to test the interaction of these inorganic nanoparticles with standard monomer reactants like styrene (PS) or methyl methacrylate (PMMA) to expand the versatility of the organic constituent. Although the interplay between the nanoscale inorganic and organic constituents is complicated, a systematic characterization of their interactions will enrich our understanding of synthesizing tunable composite microparticles.

.

References

[1]   W. Al Zoubi, M. P. Kamil, S. Fatimah, N. Nisa, and G. Ko, "Recent advances in hybrid organic-inorganic materials with spatial architecture for state-of-the-art applications," *Prog. Mater. Sci.*, p. 100663, 2020, doi: 10.1016/j.pmatsci.2020.100663.

[2]   K. Ninomiya, C. Ogino, S. Oshima, S. Sonoke, and S. Kuroda, "Ultrasonics Sonochemistry Targeted sonodynamic therapy using protein-modified TiO 2 nanoparticles," *Ultrason. - Sonochemistry*, vol. 19, no. 3, pp. 607–614, 2012, doi: 10.1016/j.ultsonch.2011.09.009.

[3]   K. Kanehira, T. Banzai, C. Ogino, N. Shimizu, Y. Kubota, and S. Sonezaki, "Properties of TiO$_2$-Polyacrylic Acid Dispersions with Potential for Molecular Recognition," *Colloids Surf. B. Biointerfaces*, vol. 64, pp. 10–15, Jul. 2008, doi: 10.1016/j.colsurfb.2007.12.018.

[4]   D. Fredj *et al.*, "Surfaces , Interfaces , and Applications A new antimony-based organic-inorganic hybrid material as electron extraction layer for efficient and stable polymer solar cells A new antimony-based organic-inorganic hybrid material as electron extraction layer f," 2019, doi: 10.1021/acsami.9b12409.

[5]   W. Al Zoubi, J. H. Min, and Y. G. Ko, "Hybrid organic-inorganic coatings via electron transfer behaviour," *Sci. Rep.*, no. March, pp. 1–15, 2017, doi: 10.1038/s41598-017-07691-x.

[6]   Y. Fink *et al.*, "A dielectric omnidirectional reflector," *Science (80-.).*, vol. 282,

no. 5394, pp. 1679–1682, Nov. 1998, doi: 10.1126/science.282.5394.1679.

[7]   J. A. Dobrowolski and S. H. C. Piotrowski, "Refractive index as a variable in the numerical design of optical thin film systems," *Appl. Opt.*, vol. 21, no. 8, p. 1502, Apr. 1982, doi: 10.1364/ao.21.001502.

[8]   H. K. Raut, V. A. Ganesh, A. S. Nair, and S. Ramakrishna, "Anti-reflective coatings: A critical, in-depth review," *Energy Environ. Sci.*, vol. 4, no. 10, pp. 3779–3804, 2011, doi: 10.1039/c1ee01297e.

[9]   B. M. Phillips and P. Jiang, *Biomimetic Antireflection Surfaces*. Elsevier Inc., 2013.

[10]   J. Moghal, S. Reid, L. Hagerty, M. Gardener, and G. Wake, "Development of single layer nanoparticle anti-re fl ection coating for polymer substrates," vol. 534, pp. 541–545, 2013, doi: 10.1016/j.tsf.2013.03.005.

[11]   A. Ramizy, Y. Al-Douri, K. Omar, and Z. Hass, "Optical Insights into Enhancement of Solar Cell Performance Based on Porous Silicon Surfaces," in *Solar Cells - Silicon Wafer-Based Technologies*, InTech, 2011.

[12]   L. Schirone, G. Sotgiu, and F. P. Califano, "Chemically etched porous silicon as an anti-reflection coating for high efficiency solar cells," *Thin Solid Films*, 1997, doi: 10.1016/S0040-6090(96)09436-9.

[13]   J. Sun *et al.*, "Biomimetic Moth-eye Nanofabrication: Enhanced Antireflection with Superior Self-cleaning Characteristic," *Sci. Rep.*, vol. 8, no. 1, pp. 1–10, 2018, doi: 10.1038/s41598-018-23771-y.

[14] "https://www.syfy.com/syfywire/why-creepy-moth-eyes-could-advance-the-next-generation-of-smartphones." .

[15] S. A. Boden and D. M. Bagnall, "Moth-Eye Antireflective Structures," *Encycl. Nanotechnol.*, pp. 1467–1477, 2012, doi: 10.1007/978-90-481-9751-4_262.

[16] V. A. Markel, "Introduction to the Maxwell Garnett approximation: tutorial," *J. Opt. Soc. Am. A*, vol. 33, no. 7, p. 1244, 2016, doi: 10.1364/josaa.33.001244.

[17] R. Q. F. Janssen, *Polymer Encapsulation of Titanium Dioxide: Efficiency, Stability and Compatibility*, no. 1995. 1994.

[18] Y. Haga, T. Watanabe, and R. Yosomiya, "Encapsulating polymerization of titanium dioxide," *Die Angew. Makromol. Chemie*, vol. 189, no. 1, pp. 23–34, 1991, doi: 10.1002/apmc.1991.051890103.

[19] M. A. M. Mballa, J. P. A. Heuts, and A. M. Van Herk, "Encapsulation of non-chemically modified montmorillonite clay platelets via emulsion polymerization," *Colloid Polym. Sci.*, vol. 291, no. 3, pp. 501–513, Mar. 2013, doi: 10.1007/s00396-012-2732-9.

[20] M. Huang, Y. Liu, G. Yang, J. Klier, and J. D. Schiffman, "Anionic Polymerization of Methylene Malonate for High-Performance Coatings," *ACS Appl. Polym. Mater.*, vol. 1, no. 4, pp. 657–663, 2019, doi: 10.1021/acsapm.8b00135.

[21] P. Classification, P. R. Stevenson, L. City, and K. Kishen, "The two tondi tullutuklandi maine," vol. 1, 2017.

[22]   S. Trevenen and P. J. Beltramo, "Gradient stretching to produce variable aspect ratio colloidal ellipsoids," *J. Colloid Interface Sci.*, vol. 583, pp. 385–393, Feb. 2021, doi: 10.1016/J.JCIS.2020.09.065.